Article

Electroviscous Effect of Water-Base Nanofluid Flow between Two Parallel Disks with Suction/Injection Effect

**Muhammad Sohail Khan [1], Sun Mei [1,*], Shabnam [1], Unai Fernandez-Gamiz [2], Samad Noeiaghdam [3,4],
Aamir Khan [5,*] and Said Anwar Shah [6]**

1   School of Mathematical Sciences, Jiangsu University, Zhenjiang 212013, China;
    sohailkhan8688@gmail.com (M.S.K.); shabnam8688@gmail.com (S.)
2   Nuclear Engineering and Fluid Mechanics Department, University of the Basque Country UPV/EHU,
    Nieves Cano 12, 01006 Vitoria-Gasteiz, Spain; unai.fernandez@ehu.eus
3   Industrial Mathematics Laboratory, Baikal School of BRICS, Irkutsk National Research Technical University,
    664074 Irkutsk, Russia; noiagdams@susu.ru
4   Department of Applied Mathematics and Programming, South Ural State University, Lenin Prospect 76,
    454080 Chelyabinsk, Russia
5   Department of Pure and Applied Mathematics, University of Haripur, Haripur 22620, Pakistan
6   Department of Basic Sciences and Islamiat, University of Engineering and Technology Peshawar,
    Peshawar 25000, Pakistan; anwarshah@uetpeshawar.edu.pk
*   Correspondence: sunm@ujs.edu.cn (S.M.); aamir.khan@uoh.edu.pk (A.K.)

Abstract: This article, investigates the behaviour of an ionized nanoliquid motion regarding heat
transmission between two parallel discs. In the proposed model, the squeezing flow of Cu-water
nanofluid with electrical potential force is analysed for studying the flow properties and an uniform
magnetic field is applied to that fluid, by taking the surface of the bottom disc porous. We have
also studied the effects of different nanomaterials on the transmission of heat through nanofluids.
Furthermore, the influence of various physical parameters in the proposed model of nanofluids flow
like volume fraction of nanomaterials, squeezing number, Hartmann number, Eckert number, and
Prandtl number are analysed and discussed quantitatively through various tables and graphs. The
system of nonlinear partial differential equations (PDE's) has been used to formulate the proposed
flow model and later converted to a set of nonlinear ODE's by mean similarity transformation.
Further, the reduced form of ODEs has been solved by Parametric Continuation Method (PCM),
which is a stable numerical scheme. The outcomes obtained from the proposed model could also
be used to analyse nanofluid flow in several fields, such as polymer processing, power transfer and
hydraulic lifts.

Keywords: nanofluid; electro-viscous fluid; Lorentz force; parametric continuation method and BVP4C

MSC: 76N17; 76N25

1. Introduction

The squeezing flow of nanoliquid in the gap of two parallel disks is used in several
industrial processes such as drilling tools, solar devices, updating punching equipment
and cooling devices. Nanoliquids differ from ordinary liquids, especially in their ther-
mophysical properties like thermal diffusivity, viscosity, and thermal conductivity. It is
currently being used in many industrial processes such as transportation, pharmaceuticals,
nuclear reactors and process involving heat and mass transfer. Many researchers have
begun to explore the barriers to using simple fluids. It came to the discussion after the
introduction of nanoliquids. That is why many research is being done on nanofluids in
terms of heat transfer.

Analysis of nanoliquid flow between two parallel squeezing discs with the same
geometry can be found in the following research articles. In the literature, the idea of

squeezing flow has been introduced for the first time by Stefan [1] . He did his research using a moderate lubrication method and analyzed Newtonian fluid using an Adhoc asymptotic approach. Von Karman [2] introduced the well-known similarity transformation technique that reduces the system of PDEs to a system of ODEs. Such systems of ODEs can be solved through various analytical and numerical methods. Engmann et al. [3] has provided the fundamental theory of squeezing flow along with its developments. It was reviewed that the squeezing flow is temporary in nature. Empirical studies have failed to provide a general correlation between the basic rheological quantities of fluid flow phenomena. Burbidge et al. [4] described the fluid flow of thin lubricating films. The fluid flow is categorised into three main types, poorly lubricated regime, slip regime and super lubricated regime. There is a strong consideration between theoretical and experimental analysis.

Ali and Butt [5]studied the influence of entropy generation in the rotating disk and concluded that the rate of squeezing fluid motion is inversely proportional to the effects of local entropy generation rate. Buongiorno [6]investigated that the flow of nanofluid via slippery effects between nanomaterials and base fluid molecules. The analysis concludes that significant slippery effects are due to thermophoresis and Brownian motion. For the critical study of nanofluid flow, the slippery and homogenous models were used simultaneously. Later on, Hayat et al. [7] studied the axisymmetric flow effects on MHD under the effect of convective boundary conditions for third-grade fluid flow. In their proposed model, they have analysed the fluid flow between two parallel discs, one fixed and the other squeezing. Nanomaterials, whether non-metallic or metallic with a diameter of less than 100 nm, are important elements of nanofluids. Experimental studies have shown that nano-fluids have maximum thermal conductivity but low emissions, thus showing significant stability when mixed with other particles. Because of these features, nano-fluids are very useful in radiators, heat exchangers and cooling electronic systems. Choi [8] concluded that blending metallic nanomaterials into base fluids increments the thermal conductivity of nanofluids. After this, many scientists have turned to nano-fluids. Rashdi et al. [9] studied MHD effects on the flow via blending alumina and copper oxide into a base fluid with a uniform magnetic field between two permeable channels.

In addition, Mustafa et al. [10] investigated the squeezing flow of viscous liquid between two parallel plates regarding mass and heat transfer, and the flow model was solved in MATHEMATICA by HAM. They noticed that the Nusselt number increments due to the increment in the values of Pr and Ec as the Nusselt number involved both Ec and Pr. Pourmehran et al. [11] numerically solved the squeezing flow model of incompressible nanoliquids by collocation and least square method to study heat and mass transfer phenomena. In their analysis, they used two parallel plates horizontally and studied the effects of various parameters such as skin friction and Nusselt number. Khilap et al. [12] investigated the motion of an incompressible liquid between two parallel plates to see the velocity, temperature and magnetic field profile. The proposed model of fluid flow has been solved using (RK-4, RK-5) numerical scheme in the shooting method. The numerical outcomes of the model solution were used to describe various flow properties and parameters such as velocity and temperature profile, nanomaterials volume fraction, Hartman number and Schmidt number. Siddiqui et al. [13] examined the hydro-magnetic effect of viscous fluid flow in the gap of two horizontal plates. The heat transfer phenomenon of nano-liquid along with magnetic field was analysed by Hatami et al. [14].

Acharya et al. [15] investigated the behaviour of squeezing nano-fluid flow of (Cu-water, Cu-kerosene) under the influence of a variable magnetic field. The proposed flow model has been solved numerically by RK-4 numerical scheme. Hussain et al. [16] analysed the flow of nano-fluid for the effect of microcirculation and concluded that microcirculation has an increasing effect on skin friction as well as heat transfer. It has been observed that Ag-water nanoliquid has a lower heat transfer rate than Ag-kerosene oil nanoliquid. Nanomaterials exist in many shapes and sizes. Ag and Cu are spherical-shaped metal nanoparticles, while single and multi-walled carbon nanotubes are tube-shaped.

A comparative study of nanoparticles in different shapes and sizes has been done by Timofeeva et al. [17] to analyse their influence on the thermal conductivity in a viscous nanofluid. They have concluded that the blade-shaped nano-particles have more thermal conductivity. Vajravelu et al. [18] analysed the flow behaviour of Ag-water and Cu-water nanofluid with respect to heat transfer and concluded that the thickness of the thermal boundary layer for Ag-water nanofluid increases more as compared to Cu-water nanofluid. In the last century, numerous studies [19] have been conducted on nanofluids in different geometries and discussed its uses in several fields such as extrusion, coolants, packaging processes and heat exchangers. Sheikholeslami et al. [20] explained asymmetrical nano-fluid flow between squeezing boundaries. It has been observed that the values of skin friction and Nusselt number for silver are higher than other nanomaterials. In addition, the Nusselt number relies heavily on nanomaterials volumetric concentration.

Electroosmotic fluid flow and electrical potential energy are usually modelled by the Poisson equation. The Poisson–Boltzmann equation has been validated by thermodynamic equilibrium, where the distribution of ions does not apply to fluid flow. Furthermore, it is considered to be a steady electroosmotic fluid through the micro-channel and is one of the most important points having an unusual effect on the convective transport of ions. This formulates the physical process with an internal electric field, so the Nernst–Planck equation can be used as a substitute for the Poisson–Boltzmann equation. Hu et al. [21] examined the electro-kinetic fluid flow in T-shaped squeezing plates. The nonlinear Poisson–Boltzmann equation for the electrokinetic surface is numerically solved to obtain the electric potential. It is used in the fluid flow where the potential force is applied at the end of the channel. The impacts of electrokinetics on the movement of fluids in a micro-channel between two parallel plates have been investigated by Mala et al. [22]. Yang et al. [23] found that the initial flow effect is due to the use of electric potential through microchannels. The flow model has been solved numerically to look at the behaviour of ion distribution and Nernst–Planck equations.

Davidson et al. [24] reviewed the error estimates in high-frequency RDF schemes with respect to interface effects and introduced a method for analysing scale interface and wave break multimedia scenes. Park et al. [25] analysed the phenomena of electrically conductive fluids and the power of electroosmotic via Poisson–Boltzmann equations where the distribution of ions is not affected by the flow of fluids. Although this is not acceptable to electroosmotic fluids flowing between two plates, there are several issues, which critically affect the temperature of concrete ions. The two equations, Nernst–Planck and Poisson–Boltzmann, have been compared for the electro-osmotic fluid flow between channels, where the ideal ionization of ions has not been specified. Rojas et al. [26] analysed the behaviour of low aggregate zeta potential and solved the flow model analytically, while a numerical solution was available. The outcomes of the model disclose that the slope of the wall surface and volumetric flow rate in the microchannel are increasing. Thiyagarajan et al. [27] scrutinized the pleural effusion process in the lung wall as obstruction of the pleural cavity. The reversal process of the lung and chest wall causes the accumulation of pleural fluid in the pleural space. Parietal lymphatic dilation is caused by an increase in pleural liquid. This approach has been introduced to acquire new outcomes of respiratory tract infections, and has been injected into an unstable natural and forced convection transport flow of neural pleural fluid in two types of vertical porous spaces, which was later researched. M. K. Alam et al. [28] examined the impacts of mass and heat transfer at the transient squeezing flow of viscid liquid in the presence of a variable magnetic field. Bilal et al. [29] and Khoshroi [30] researched advances in various technologies like power engineering and microelectronics based on the development of efficient cooling systems. This process involves the use of fins of considerably variable geometry within cavities to increment the heat dissipation from the heat generation process. Since fins are thought to play an effective role in enhancing heat transfer, the aim of the ongoing research is to examine the effects of different parameters on energy transfer as well as the energy transmission in fins embedded in the cavities.

Rizwan et al. [31] investigated the behaviour of heat transfer in the squeezing flow of nanofluid using water-based copper nanomaterials in the gap of two parallel discs with injection/suction effects. As metallic components are greatly influenced by the magnetic field due to the involvement of MHD effects, it is applied orthogonally to the surface, and the bottom disc usually taken is porous. Khan et al. [32,33] examined the Poisson-Boltzmann model, which derives from the hypothesis of thermodynamic equilibrium on the condition that the distribution of ions will not be affected by the flow of liquid. Nevertheless, it is considered a reasonable hypothesis for the stable flow of electroosmotic fluid through straight micro-channels, there are some key situations where the convective transport of ions has extraordinary effects. In all these situations, the Nernst-Planck equation must be used in spite of the Poisson-Boltzmann equation to formulate the electric field in the domain. Khan et al. [34–37] analysed the influence of variable magnetic fields in the flow of hybrid nanoliquids to see the improvement in the heat transfer rate. The purpose of their study was to see the influence of nanofluid (Cu-H$_2$O) between two parallel discs under the influence of a variable magnetic field.

From the above literature review, It is noticed that the investigation of nanofluids by dissolving copper nanomaterial with a changeable magnetic field in the gap of two parallel porous discs so far has not been considered. In addition, the impact of variable magnetic fields on the mass and heat transfer in such flow of nanofluid is a novelty in current research. This type of nano-fluid flow is very important in many industrial and engineering processes. In this article, we are going to analyse the fluid flow in the presence of ions. Velocity profile, temperature profile, Nusselt number and skin frictions are calculated, which explain the flow properties of the proposed flow model. In addition, the impacts of variable magnetic fields in the nanofluid flow of copper nanomaterials are analysed to see the enhancement in heat transfer rate. The governing equations of the proposed hybrid nanofluid are modelled under certain assumptions and solved numerically by (parametric continuation method) in MATLAB. The numerical outcomes of several emerging parameters like skin frictions, Nusselt number, etc., are discussed using various tables and graphs Figure 1.
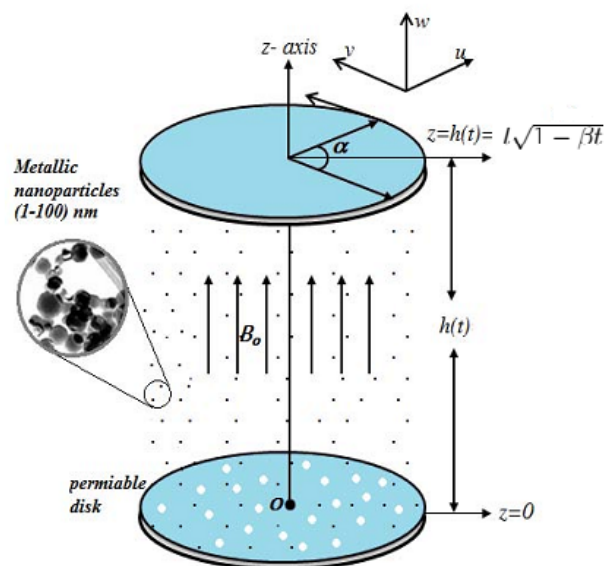
Figure 1. Geometry of the problem.

2. Formulation

An unsteady, incompressible, electro-viscous nanofluid is considered between the circular space of two squeezing disks. The two discs apart from one another by $h(t) = l\sqrt{1 - \beta t}$, where, l denotes the length, the two discs will be parallel if $t = 0$. Subsequently, we suppose that the fluid has symmetric positive $(+)$ and negative $(-)$ ions along with

valencies of $z_+ = -z_- = z = 1$ and n_o in the bulk ions concentration of ionic species. Electrokinetic fluid flows having ionic species are explained by the Navier–Stokes equations through the inclusion of uniform magnetic field and electrical body force terms. The model involving these equations is further updated through the inclusion of Poisson equation, Nernst–Planck equation and charge distribution for the conversion of every ion species.

The mathematical modelling of the proposed nanofluid flow as follow [27–29]:

Continuity equation:

$$\nabla.\vec{U} = 0, \tag{1}$$

The updated momentum equation through electroviscous and magnetic effect [25,31]:

$$\frac{\partial \vec{U}}{\partial t} + (\vec{U}.\nabla)\vec{U} = -\frac{1}{\rho_{nf}}\nabla P + \frac{\mu_{nf}}{\rho_{nf}}\nabla^2\vec{U} - \frac{\mu_{nf}^2}{\rho_{nf}^2}BK^2(n^+ - n^-)\nabla V - \frac{\sigma}{\rho_{nf}\mu_e}(\vec{H} \times \vec{U}) \times \vec{H} \tag{2}$$

The Poisson equation [25]:

$$\nabla^2 V = \frac{-1}{2}K^2(n^+ - n^-) \tag{3}$$

The Nernst–Planck equations [25]:

$$\frac{\partial n_+}{\partial t} + \nabla.(\vec{U}n_+) = \frac{\mu_{nf}}{\rho_{nf}S_c}(\nabla^2 n_+ + \nabla.(n_+\nabla V)) \tag{4}$$

$$\frac{\partial n_-}{\partial t} + \nabla.(\vec{U}n_-) = \frac{\mu_{nf}}{\rho_{nf}S_c}(\nabla^2 n_- + \nabla.(n_-\nabla V)) \tag{5}$$

and the Equations of energy [31]:

$$\frac{\partial T}{\partial t} + \vec{U}.\nabla T = \frac{k_{nf}}{(\rho C_p)_{nf}}\nabla^2 T + \frac{1}{(\rho C_p)_{nf}}tra(\tau.L) \tag{6}$$

where H the magnetic field, U velocity of the fluid, P fluid pressure, ρ_{nf} nano-liquid density, σ fluid electrical conductivity, Sc Schmidt number, T fluid temperature profile, κ_{nf} nanoliqui thermal conductivity, V total local electrical potential induced, K^2 is the inverse Debye constant, $(\rho C_p)_{nf}$ specific heat of the nanofluid, $(\rho C_p)_f$ specific heat of the base fluid, μ_{nf} nanoliquid kinematic viscosity, n^+, n^- are the anions and cations, $\tau = \mu_f A_1$ Shear stress, μ_f the dynamic viscosity of the flow, $A_1 = L + L^T$ and $L = \Delta U$, respectively.

Nanofluids are defined as [31]:

$$\rho_{nf} = \rho_f(1 - \phi + \phi\frac{\rho_s}{\rho_f}), \quad \mu_{nf} = (1 - \phi)^{-2.5}\mu_f,$$
$$\frac{\kappa_{nf}}{\kappa_f} = \frac{\kappa_s + 2k_f - 2\phi(\kappa_f - \kappa_s)}{\kappa_s + 2k_f + \phi(\kappa_f - \kappa_s)} \quad and \quad \frac{(\rho C p)_{nf}}{(\rho C p)_f} = 1 - \phi + \phi\frac{(\rho C p)_s}{(\rho C p)_f}, \tag{7}$$

where κ_{nf} and κ_s are the base fluid and solid fraction thermal conductivities, respectively, and ϕ is the volume fraction of the solid nanomaterials.

Boundary Conditions

The boundary conditions of the proposed model are taken as follow:

$$u = 0, \; w = -\frac{dh}{dt}, \; V = \frac{r^2}{2l(1 - \beta t)}, \; n^- = 0, \; n^+ = 0, \; T = T_u \quad at \quad z = h(t)$$
$$u = 0, \; w = \frac{-w_o}{\sqrt{1 - \beta t}}, \; V = 0, \; T = T_l, \; n^+ = \frac{\beta}{1 - \beta t}, \; n^- = \frac{\beta}{1 - \beta t}, \quad at \quad z = 0 \tag{8}$$

For converting PDEs into ODEs, the following similarity variables [31] have been used,

$$u = \frac{\beta r}{2(1 - \beta t)} f'(\eta), \quad w = -\frac{\beta l}{\sqrt{1 - \beta t}} f(\eta), \quad n_+ = \frac{\beta \mu_f m(\eta)}{\rho_f (1 - \beta t)}, \quad n_- = \frac{\beta \mu_f n(\eta)}{\rho_f (1 - \beta t)},$$

$$\theta(\eta) = \frac{T - T_u}{T_l - T_u}, \quad V = \frac{r^2 P(\eta)}{l^2 (1 - \beta t)}, \quad \text{where} \quad \eta = \frac{z}{l \sqrt{1 - \beta t}} \tag{9}$$

So, Equation (1) is satisfying automatically and the remaining Equations (2)–(6) takes the following form.

$$f^{iv} - \frac{\rho_{nf}}{\mu_{nf}} S(\eta f''' + 3 f'' - f f''') - \frac{1}{\mu_{nf}} M f''$$

$$+ \frac{\mu_{nf}}{\rho_{nf}} 2 B K^2 (P'm + P m' - P n' - P'n) = 0, \tag{10}$$

$$P'' + 4P - S K_1 K^2 (n - m) = 0, \tag{11}$$

$$m'' - \frac{\rho_{nf}}{\mu_{nf}} S S_c (\eta m' + 2m - 2m' f) + 2mP + \delta P'm' - (4Pm - S K^2 K_1 (m^2 - mn)) = 0, \tag{12}$$

$$n'' - \frac{\rho_{nf}}{\mu_{nf}} S S_c (2n + \eta n' - 2n' f) - 2nP - \delta P'n' + (4Pn + S K^2 K_1 (mn - n^2)) = 0, \tag{13}$$

$$\theta'' - \frac{\kappa_{nf}}{\kappa_f} Pr \big(\frac{(\rho Cp)_{nf}}{(\rho Cp)_f} S(\eta \theta' - \theta' f) - \mu_{nf} Ec (6 f'^2 + f''^2) \big) = 0. \tag{14}$$

The boundary conditions in transform form as follow:

$$f'(0) = 0, \quad f(0) = A, \quad P(0) = 0, \quad m(0) = 1, \quad n(0) = 1, \quad \theta(0) = 1,$$

$$f(1) = 0.5, \quad f'(1) = 0, \quad P(1) = 1, \quad m(1) = 0, \quad n(1) = 0, \quad \theta(1) = 0, \tag{15}$$

where $Sc = \frac{\nu}{D}$ Schmidt number, $S = \frac{\beta l^2}{2\nu}$ squeeze number, $Pr = \frac{\nu_f (\rho Cp)_f}{\kappa_f}$ Prandtl number, $Ec = \frac{1}{(Cp)_f (T_0 - T_h)} \big(\frac{\beta r}{2(1 - \beta t)} \big)^2$ Eckert number, $B = \frac{\rho k^2 T^2 \varepsilon_0 \varepsilon}{2 z^2 e^2 \mu^2}$ is fixed at a specified temperature, $K_1^2 = \frac{2 z^2 e^2 l^2 n_0}{\varepsilon_0 \varepsilon k_b T}$ the dimensionless inverse of Debye length and $M = \sqrt{\frac{l^2 \sigma B_0^2}{\rho_f \mu_e}}$ Magnetic Parameter. The parameter $A = \frac{w_o}{\beta l} > 0$ corresponds to suction and $A = \frac{w_o}{\beta l} < 0$ corresponds to injection of fluid from the lower disk.

Nusselt number and skin friction are the desired physical quantities, which can be written as follow:

$$C_f = \frac{\mu_{nf}}{\rho_{nf} \big(\frac{\beta r}{2(1 - \beta t)} \big)^2} \big(\frac{\partial u_r}{\partial z} \big)_{z = h(t)}, \quad N_u = -\frac{\kappa_{nf} \big(\frac{\partial T}{\partial z} \big)_{z = h(t)}}{k_f (T_0 - T_h)}, \tag{16}$$

In case of Equation (16), we get

$$\frac{r}{\sqrt{1 - \beta t}} SC_f = \frac{\mu_{nf}}{\rho_{nf}} f''(1), \quad -\frac{\kappa_{nf}}{\kappa_f} \theta'(0) = N_u l \sqrt{1 - \beta t}. \tag{17}$$

3. Numerical Solution by PCM

This section explains the procedure for the selection of an optimal value of the continuation parameters along with the practical implementation of PCM [32,33], which is used for the solution of non-linear ODEs in (10)–(14) with predetermined boundary conditions (15).

- **First order of ODE**
  We consider the following for reducing Equations (10)–(14) into first-order ODEs:

$$
\begin{aligned}
f &= Y_1, \quad f' = Y_2, \quad f'' = Y_3, \quad f''' = Y_4 \\
P &= Y_5, \quad P' = Y_6, \quad m = Y_7, \quad m' = Y_8 \\
n &= Y_9, \quad n' = Y_{10}, \quad \theta = Y_{11}, \quad \theta' = Y_{12}
\end{aligned}
\tag{18}
$$

By using these transformations in Equations (10)–(14), we get,

$$
\begin{aligned}
Y_4' ={}& \frac{\rho_{nf}}{\mu_{nf}} S(3Y_3 + \eta Y_4 - Y_1 Y_4) + \frac{1}{\mu_{nf}} M Y_3 \\
&- \frac{\mu_{nf}}{\rho_{nf}} 2BK^2(Y_5 Y_8 + Y_6 Y_7 - Y_6 Y_9 - Y_5 Y_{10}),
\end{aligned}
\tag{19}
$$

$$
Y_6' = -4Y_5 - SK^2 K_1(Y_7 - Y_9),
\tag{20}
$$

$$
\begin{aligned}
Y_8' ={}& \frac{\rho_{nf}}{\mu_{nf}} S_c S(\eta Y_8 + 2Y_7 - 2Y_1 Y_8) - 2Y_5 Y_7 - \delta Y_8 Y_8 \\
&+ \delta(4Y_5 Y_7 - SK^2 K_1(Y_7^2 - Y_7 Y_9)),
\end{aligned}
\tag{21}
$$

$$
\begin{aligned}
Y_{10}' ={}& \frac{\rho_{nf}}{\mu_{nf}} S_c S(\eta Y_{10} + 2Y_9 - 2Y_1 Y_{10}) + 2Y_5 Y_9 + \delta Y_6 Y_{10} \\
&- \delta(4Y_5 Y_9 + SK^2 K_1(Y_7 Y_9 - Y_9^2)),
\end{aligned}
\tag{22}
$$

$$
Y_{12}' = \frac{(\rho Cp)_{nf}}{(\rho Cp)_f} \frac{\kappa_f}{\kappa_{nf}} SPr(\eta Y_{12} - Y_1 Y_{12}) - \frac{\kappa_f}{\kappa_{nf}} \mu_{nf} PrEc(6Y_2^2 + \delta Y_3^2),
\tag{23}
$$

and the boundary conditions becomes

$$
\begin{aligned}
&Y_2(0) = 0, \quad Y_1(0) = A, \quad Y_2(1) = 0, \quad Y_1(1) = \frac{1}{2}, \quad Y_5(0) = 0, \quad Y_5(1) = 1, \\
&Y_7(0) = 1, \quad Y_7(1) = 0, \quad Y_9(0) = 1, \quad Y_9(1) = 0, \quad Y_{11}(0) = 1, \quad Y_{11}(1) = 0,
\end{aligned}
\tag{24}
$$

- **Introduction of the q-Parameter**
  The ODEs in the q-parameter group is explained through the introduction q-parameter in Equations (19)–(23) and we have,

$$
\begin{aligned}
Y_4' ={}& \frac{\rho_{nf}}{\mu_{nf}} S(3Y_3 + \eta Y_4 - Y_1(Y_4 - 1)q) + \frac{1}{\mu_{nf}} M Y_3 \\
&- \frac{\mu_{nf}}{\rho_{nf}} 2BK^2(Y_5 Y_8 + Y_6 Y_7 - Y_6 Y_9 - Y_5 Y_{10}),
\end{aligned}
\tag{25}
$$

$$
Y_6' = -4Y_5 - SK^2 K_1(Y_7 - Y_9 + Y_6 - (Y_6 - 1)q),
\tag{26}
$$

$$
\begin{aligned}
Y_8' ={}& \frac{\rho_{nf}}{\mu_{nf}} S_c S(\eta Y_8 + 2Y_7 - 2Y_1(Y_8 - 1)q) - 2Y_5 Y_7 - \delta Y_8 Y_8 \\
&+ \delta(4Y_5 Y_7 - SK^2 K_1(Y_7^2 - Y_7 Y_9)),
\end{aligned}
\tag{27}
$$

$$
\begin{aligned}
Y_{10}' ={}& \frac{\rho_{nf}}{\mu_{nf}} S_c S(\eta Y_{10} + 2Y_9 - 2Y_1(Y_{10} - 1)q) + 2Y_5 Y_9 + \delta Y_6 Y_{10} \\
&- \delta(4Y_5 Y_9 + SK^2 K_1(Y_7 Y_9 - Y_9^2)),
\end{aligned}
\tag{28}
$$

$$Y'_{12} = \frac{(\rho Cp)_{nf}}{(\rho Cp)_f} \frac{(\kappa_f}{\kappa_{nf}} SPr(\eta Y_{12} - Y_1(Y_{12} - 1)q) - \frac{\kappa_f}{\kappa_{nf}} \mu_{nf} PrEc(6Y_2^2 + \delta Y_3^2). \tag{29}$$

- **Differentiation by q, reaches at the following system w.r.t the sensitivities to the parameter-q**
  Differentiating the Equations (25)–(29) w.r.t by q

$$D'_1 = H_1 D_1 + E_1 \tag{30}$$

  where H_1 is the coefficient matrix, E_1 is the remainder and $D_1 = \frac{dY_i}{d\tau}$, $1 \leq i \leq 12$.

- **Cauchy Problem**

$$D_1 = P_1 + A1V1, \tag{31}$$

  where P_1 and $V1$ are vector value functions.

$$E_1 + H_1(A1V1 + P_1) = (A1V1 + P_1)' \tag{32}$$

  and left the boundary conditions.

- **Using by Numerical Solution**
  An absolute scheme is used to solve the problem,

$$\frac{V1^{i+1} - V1^i}{\triangle\eta} = H_1 V1^{i+1} \tag{33}$$

$$\frac{P^{i+1} - P^i}{\triangle\eta} = H_1 P^{i+1} + E_1 \tag{34}$$

- **Taking of the corresponding coefficients**
  For the solution of the ODEs, given boundaries are commonly used for q_i, where $1 \leq i \leq 12$, but it is needed to apply $D_2 = 0$, which looks in matrix form as given,

$$L_1.D_1 = 0 \quad \text{or} \quad L_1.(A1V1 + P_1) = 0 \tag{35}$$

  where $A1 = \frac{-L_1.P_1}{L_1.V1}$.

4. Results and Discussions

To investigate the flow of nanofluid regarding heat and mass transfer under the effects of ions distribution, we have displayed the numerical outcomes of different flow properties graphically like radial velocity $f'(\eta)$, axial velocity $f(\eta)$, positive ions $m(\eta)$, negative ions $n(\eta)$, Poisson variable $P(\eta)$, and heat transfer $\theta(\eta)$ for the different values of flow parameters such as squeezing number, Hartman number, the volume fraction of nanomaterials and suction/injection parameter A. Most of the flow properties of the proposed model are described through the various graphs in the prescribed domain $0 \leq \eta \leq 1$. Figures 2–10 are plotted to analyse the impact of squeezing nanofluids flow with variable magnetic field in the presence of ions distribution.
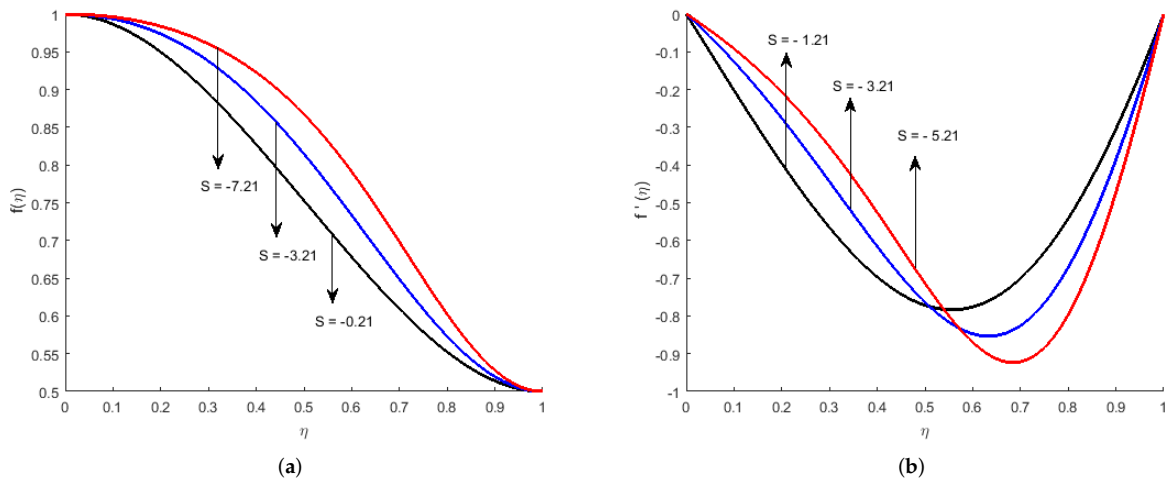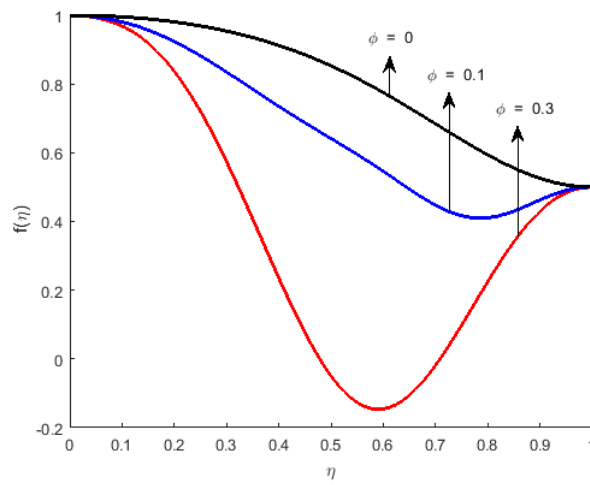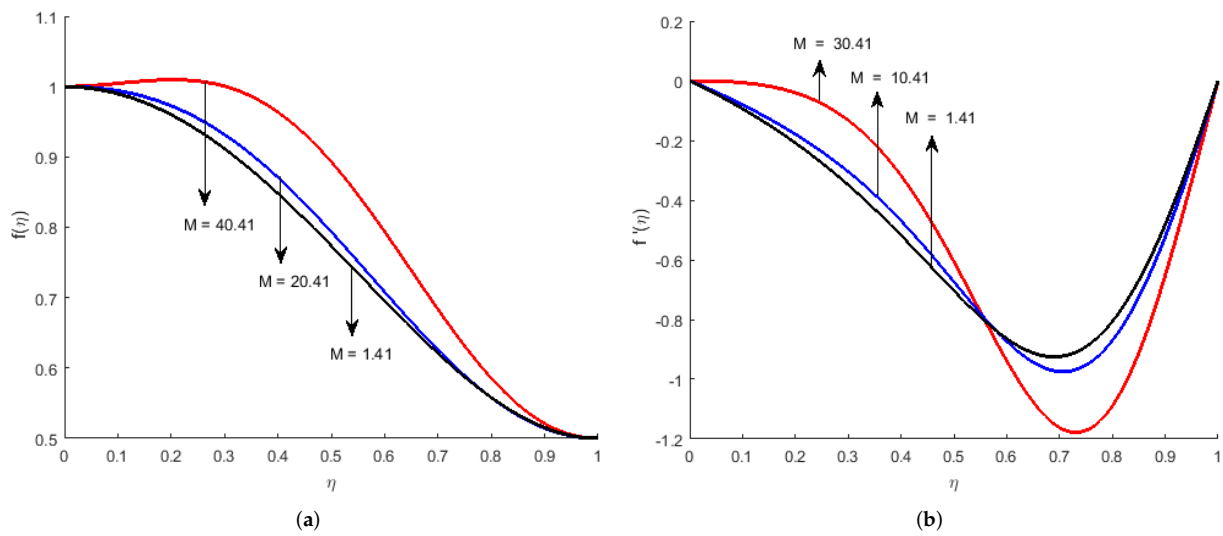
Figure 2. Impact of (**a**) $f(\eta)$ and (**b**) $f'(\eta)$ for squeeze parameter and fixed values of $M = 0.41, K = 0.20, B = 1.41, K_1 = 0.50, \delta = 1, Sc = 1.50, Pr = 1.50, Ec = 0.50.$
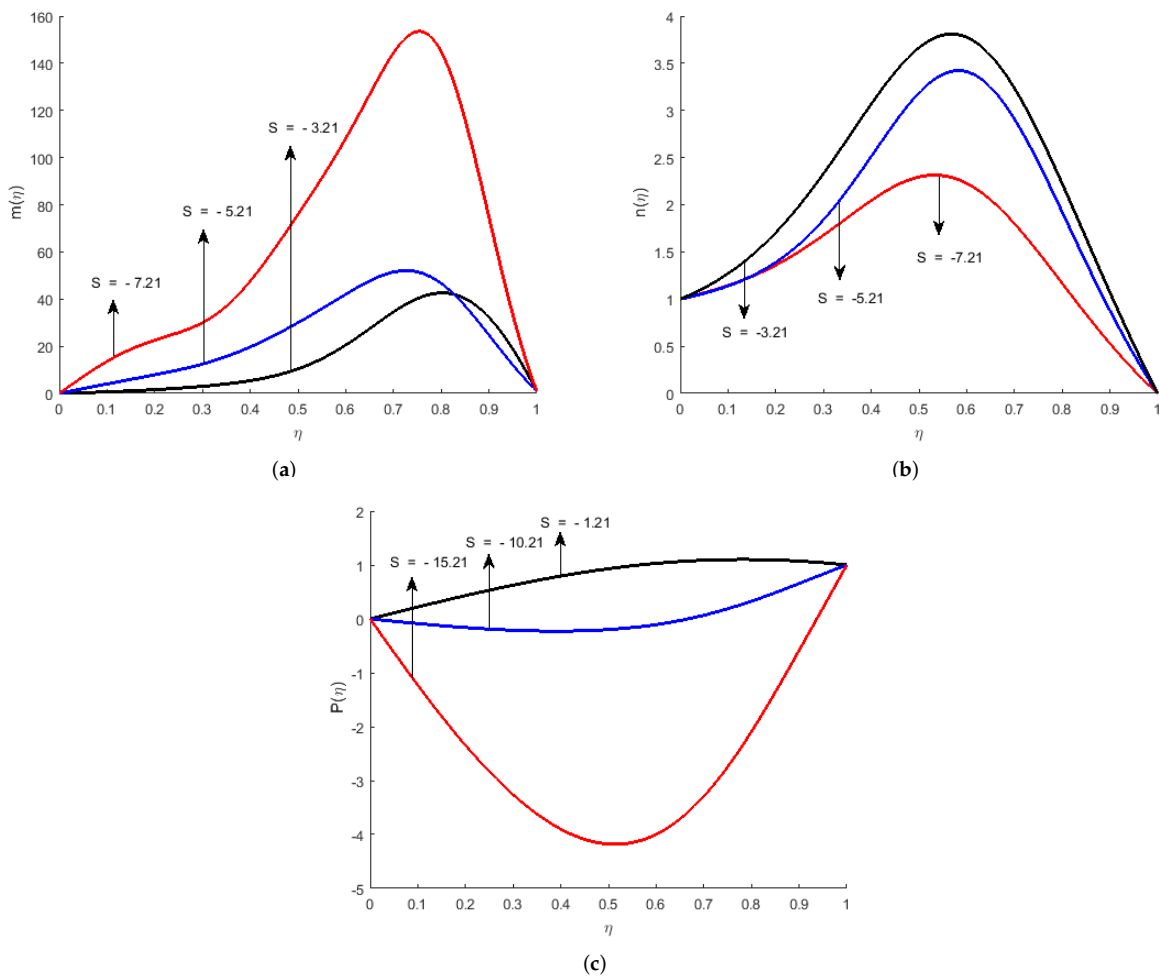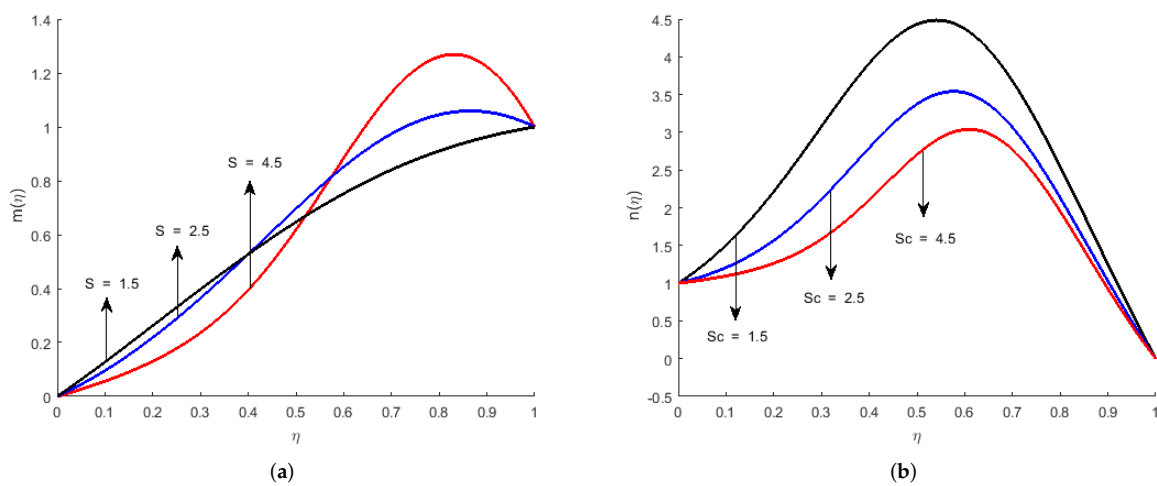

Figure 3. Impact of (**a**) $m(\eta)$, (**b**) $n(\eta)$ and (**c**) $P(\eta)$ for squeeze parameter and fixed values of $B = 1.41, M = 0.41, K = 2.20, Sc = 1.5, K_1 = 0.50, \delta = 1.0, Pr = 1.50, Ec = 0.50.$
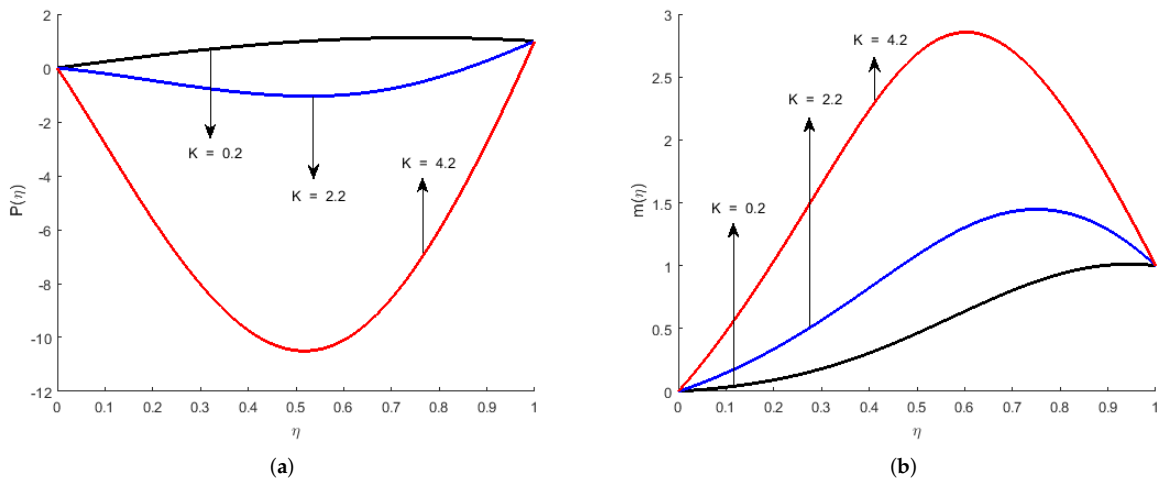
Figure 4. Impact of $f(\eta)$ for nanoparticle Φ and fixed values of $M = 0.41, S = -8.20,$ $B = 1.40, K = 0.20, Sc = 1.50, K_1 = 0.50, \delta = 1.0, Pr = 1.50, Ec = 0.50.$

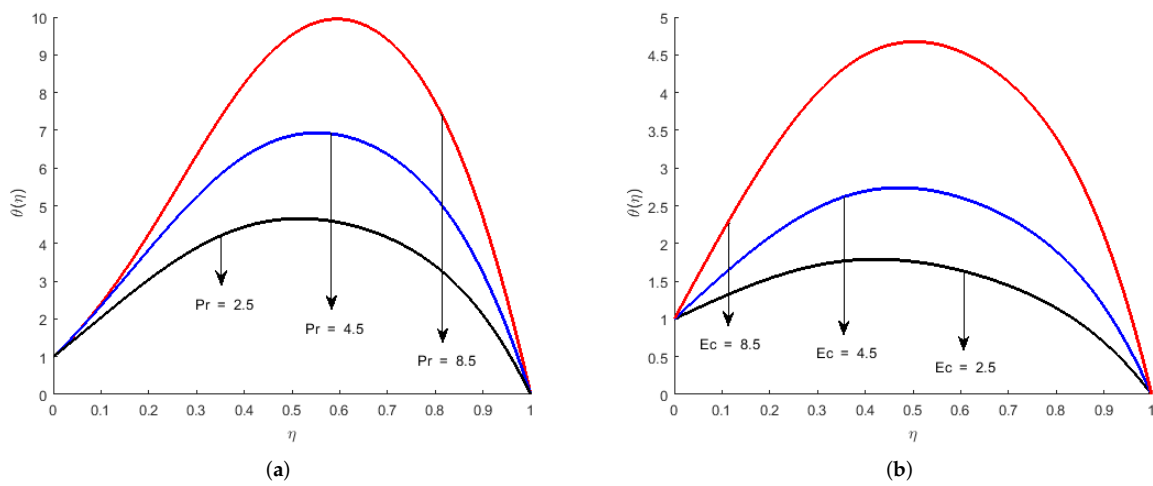**Figure 5.** Impact of (**a**) $f(\eta)$ and (**b**)$f'(\eta)$ for magnetic parameter and fixed values of $B = 1.41, S = -1.21, K = 0.20, Ec = 0.50, Sc = 1.50, K_1 = 0.50, \delta = 1.0, Pr = 1.50.$
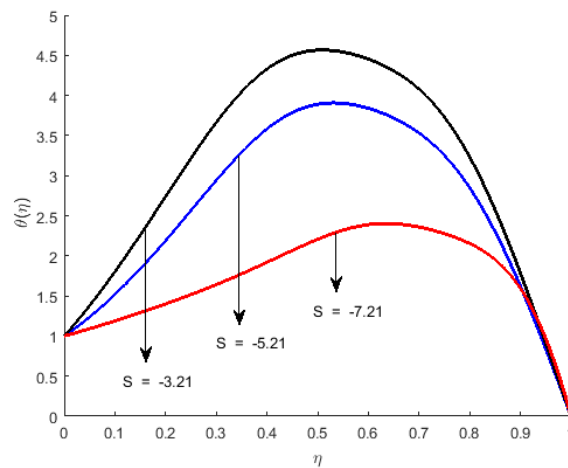

Figure 6. Impact of (**a**) $m(\eta)$ and (**b**) $n(\eta)$ for Schmidt number, Debye length parameter and fixed values of $K = 1.20, S = -2.20, B = 1.40, M = 0.41, K_1 = 0.50, \delta = 1.0, Pr = 1.50, Ec = 0.50.$

Figure 7. Impact of (**a**) $P(\eta)$ and (**b**) $m(\eta)$ for Debye length parameter and fixed values of $S = -3.21, Sc = 2.50, B = 1.40, M = 0.40, K_1 = 0.50, \delta = 1.0, Pr = 1.50, Ec = 0.50$.

Figure 8. Impact of $\theta(\eta)$ for (**a**) Prandtl number, (**b**) Eckert number and fixed values of $K = 0.20, B = 1.41, M = 0.40, K_1 = 0.50, \delta = 1.0$.

Figure 9. Impact of $\theta(\eta)$ for squeeze parameter and fixed values of $K = 0.20, B = 1.40, M = 0.40, K_1 = 0.50, \delta = 1.0, Pr = 1.50, Ec = 0.50$.

(a)   **(b)**
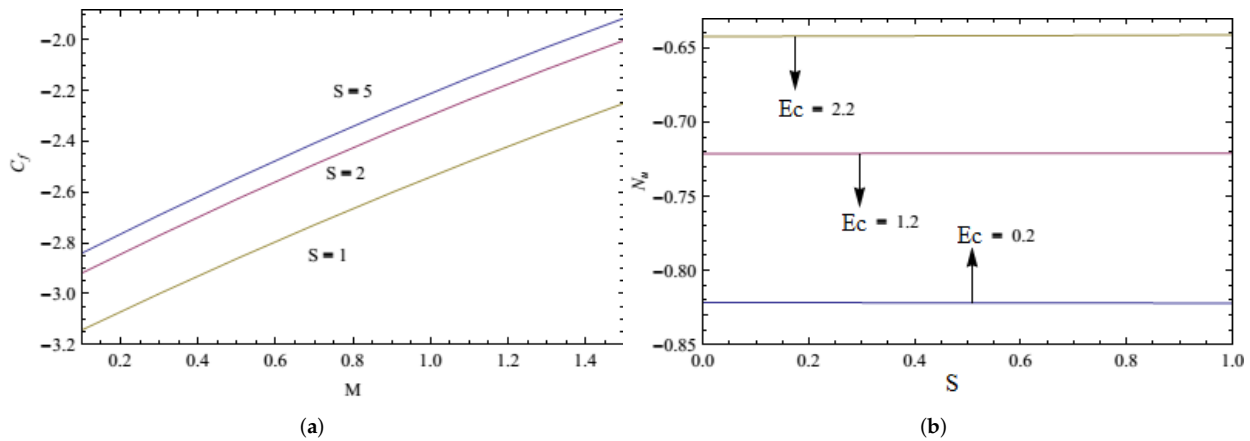
Figure 10. Impact of (**a**) Skin friction and (**b**) Nusselt number for squeeze parameter and Eckert number and fixed values of $B = 1.41, K_1 = 0.50, K = 0.20, \delta = 1.0, Pr = 1.50$.

Tables 1–3 illustrate the convergence of a numerical scheme (BVP4C) with respect to Nusselt number and skin friction for different values of the physical parameters ϕ, S and M. It has been noticed that a rise in the volume fraction of the nanoparticles ϕ raises the convergence of the scheme for the skin friction and Nusselt number under the influence of suction/injection.

Table 1. The thermophysical properties of water and nanoparticles.

	ρ	C_p	κ	Pr
Water	997.1	4179	0.613	6.2
Ethylene glycol	1115	2430	0.253	203.63
Copper	8933	385	401	

Table 2. Comparison of the numerical outcomes of skin friction for water-base Cu-nanomaterials for different values of physical parameters ϕ, S and M with suction parameter $A = 1$.

	S = 0.50				**M = 2.0**			
	Present		[31]		Present		[31]	
ϕ	$M = 0$	$M = 1.0$	$M = 0$	$M = 1.0$	$S = 0$	$S = 0.50$	$S = 0$	$S = 0.50$
0	3.05495	3.10534	3.05499	3.10533	3.09866	3.15497	3.09860	3.15494
0.1	4.24586	4.29956	4.24585	4.29957	4.24490	4.35265	4.24498	4.35268
0.2	4.57348	4.61663	4.57345	4.61660	4.53510	4.65933	4.53513	4.65937

Table 3. Comparison of the numerical results of Nusselt number for water-base and Cu nanoparticle for different values of physical parameters ϕ, S and M with suction parameter $A = 1.0$.

	S = 0.50				**M = 2.0**			
	Present		[31]		Present		[31]	
ϕ	$M = 0$	$M = 1.0$	$M = 0$	$M = 1.0$	$S = 0$	$S = 0.50$	$S = 0$	$S = 0.50$
0	1.40578	1.40640	1.40576	1.40647	1	1.40718	1	1.40710
0.1	1.73460	1.73524	1.73466	1.73521	1.33168	1.73579	1.33164	1.73574
0.2	2.14381	2.14425	2.14388	2.14428	1.74575	2.14460	1.74572	2.14467

Figures 2a,b and 3a–c illustrates the impacts of various emerging parameters of the squeezing nanoliquid motion on the velocity profile, Poisson distribution and ions distribution. It has been noticed from Figure 2a,b that the axial velocity $f(\eta)$ is always rising due to a rise in the volume fraction of nanomaterials. In addition, the axial velocity in the vicinity

of the disc is also uniform due to the volume fraction of nanomaterials. It has also been observed that the incrementing value of the squeezing parameter causes increments axial velocity. Similarly, an increment in magnetic and suction parameters increases the radial velocity profile $f'(\eta)$ when it passes through the central area ($\eta > 0.5$), then it begins to decrease as the injection effect dominates the squeezing parameter and becomes parabolic. Figure 3a–c is plotted to explain the influence of the squeezing parameter on the ions and Poisson distributions. It has been noticed that the rise in the squeezing parameter S, increments the $m(\eta)$ profile, and decrements both $n(\eta)$ and $P(\eta)$ profiles. The maximum fluctuations in these profiles are observed in the vicinity of the bottom disc as shown in Figure 3a, and decline has been noticed in the centre of the fluid domain as displayed in Figure 3b,c.

Figure 4 is plotted to see the effect of axial velocity for η using different values of nanomaterials volume faction in the domain $S < 0$. It has been noticed that the fluid velocity approaching maximum level due to a rise in ϕ in the domain $S < 0$. The reason behind this phenomenon is that when two discs move towards each other under the influence of increasing volume fraction of nanomaterials, resulting in more collision between molecules and with the boundary surface of the disc, which Increments the friction force in the fluid, as a result of which the velocity of fluid movement declines throughout the domain. In addition, an increment in the concentration of nanoparticles leads to reduce the velocity profile parabolically. Figure 5a,b illustrates the impact of Hartmann number on $f(\eta)$ and $f'(\eta)$ profiles, showing that the axial velocity begins to increase due to a rise in the value of the squeezing parameter M. Furthermore, it has been observed that the axial velocity gradually augments as the value of the squeezing parameter M rises. Figure 5b illustrates that an increment in M increments the radial velocity then declines when it passes through the central area.

Figure 6a is plotted to see the impact of squeezing parameter S on the ions distributions $m(\eta)$ and $n(\eta)$ in the domain $S < 0$. It signifies that an increment in the squeezing parameter decrements the cation distribution due to a decline in the radius of the ions that lose electrons in the domain $0 \leq \eta \leq 0.55$. This is true for electrically conducting liquids that move under the influence of a uniform magnetic field, which slows down the movement of liquids within the boundary layer area. In the case of $\eta > 0.56$, the opposite effect has been observed. In addition, it has been noticed that the ionization profile declines with an increment in Sc due to an increase in the size of the ionic radius that receives electrons, as shown in Figure 6b. Figure 7a is plotted to illustrate the effect of K at Poisson distribution, which shows that Poisson distribution is reducing in the middle of the fluid domain due to a rise in K, as the electrons are moving opposite to the direction of the electric field. Figure 7b is plotted to study the influence of K at cation distribution. It reveals that cation distribution is getting stronger for the fluid flow from the lower disc to the upper disc due to a rise in K, in this way, the cations profile increases as K increases. Figure 8a,b reveal the impacts of Ec and Pr on the heat transfer, and it has been observed that an increment in Pr and Ec causes a constant increase in the temperature of the fluid. As a resistance force, it slows down the movement of particles, in this way, temperature rises, which increases the heat transmission. The temperature profile is an augmenting function of Pr due to diffusivity and kinematic viscosity, which rises due to a rise in the value of Pr and Ec. Figure 9 is sketched to study the impact of squeezing parameter S on the heat transfer, it signifies that the increase in the squeezing parameter S declines heat diffusion, and hence the temperature profile reduces. The numerical outcomes of the Nusselt number and skin friction coefficient acquired from the solution of the proposed flow model are plotted in Figure 10, it reveals a rise in the squeezing number and Eckert number augments skin friction and Nusselt number.

5. Concluding Remarks

In this article, the electroviscous phenomena of water-based nanoliquid motion under the influence of suction/injection has been formulated through Navier–Stokes equation, energy equation, Nernst–Planck and Poisson equations, and subsequently reduced into a highly nonlinear system of ODE's using similarity transformation. The system of nonlinear ODE's have been solved through a robust numerical scheme is known as the Parametric Continuation Method (PCM). From the numerical outcomes of the proposed flow model, the following conclusions are drawn:

- Radial velocity $f'(\eta)$ is rising due to a rise in the volume fraction of the nanomaterials.
- It has been noticed that the radial velocity increment is due to increase in S and vice-versa, the axial velocity profile decrements due to the increase in magnetic and suction parameters.
- It has been concluded that a rise in S leads to an increase in $m(\eta)$ and a decrease in $n(\eta)$ and $P(\eta)$, and these profiles show maximum fluctuation close to the bottom disc.
- The rationale behind this phenomenon is that when two discs move towards each other or the volume fraction of nanomaterials rise, resulting in more collision between the volume fraction of nanomaterials and with the surface boundary of the disc.
- It has been observed that the positive ions reduce as the squeezing number rises because the size of the ionic radii decrements and the electron losses in the region $0 \le \eta \le 0.55$.

Author Contributions: Formal analysis, S.A.S.; Investigation, M.S.K.; Methodology, S.; Supervision, S.M.; Writing—review and editing, U.F.-G., S.N. and A.K. All authors have read and agreed to the published version of the manuscript.

Institutional Review Board Statement: Not applicable.

Informed Consent Statement: Not applicable.

Data Availability Statement: Not applicable.

Conflicts of Interest: The authors declare no conflict of interest.

References

1. Stefan, M.J. Versuch über die scheinbare adhäsion. *Akad. Wiss.-Math.-Naturwissenschaftliche* **1874**, *69*, 713–721.
2. Karman, T.V. Uber laminare und turbulente Reibung. *Angew. Math. Mech.* **1921**, *1*, 1233–1255. [CrossRef]
3. Engmann, J.; Servais, C.; Burbidge, A.S. Squeeze flow theory and applications to rheometry. *J. Non-Newton. Fluid Mech.* **2005**, 132, 1–27. [CrossRef]
4. Burbidge A.S., Servais C. Squeeze flows of apparently lubricated thin films. *J. Non-Newton. Fluid Mech.* **2004**, *124*, 115–127. [CrossRef]
5. Butt, A.S.; Ali, A. Analysis of entropy generation effects in unsteady squeezing flow in a rotating channel with lower stretching permeable wall. *J. Taiwan Inst. Chem. Engin.* **2015**, *48*, 8–17. [CrossRef]
6. Buongiorno, J. Convective transport in nanofluids. *J. Heat Transf.* **2006**, *128*, 240–250. [CrossRef]
7. Hayat, T.; Nazar, H.; Imtiaz, M.; Alsaedi, A.; Ayub, M. Axisymmetric squeezing flow of third grade fluid in presence of convective conditions. *Chin. J. Phys.* **2017**, *55*, 738–754. [CrossRef]
8. Choi, S.U.S.; Eastman, J.A. Enhancing thermal conductivity of fluids with nanoparticles. *Dev. Appl. Non-Newton. Flows* **1995**, *231*, 99–105.
9. Rashidi, M.M.; Reza, M.; Gupta, S. MHD stagnation point flow of micropolar nanofluid between parallel porous plates with uniform blowing. *Powder Technol.* **2016**, 301, 876–885. [CrossRef]
10. Mustafa, M.; Hayat, T.; Obaidat, S. On heat and mass transfer in the unsteady squeezing flow between parallel plates. *Meccanica* **2012**, *47*, 1581–1589. [CrossRef]
11. Pourmehran, O.; Rahimi-Gorji, M.; Gorji-Bandpy, M.; Ganji, D.D. Analytical investigation of squeezing unsteady nanofluid flow between parallel plates by LSM and CM. *Alex. Eng. J.* **2015**, *54*, 17–26. [CrossRef]

12. Singh, K.; Sawan, K.R.; Kumar, A. Heat and Mass Transfer on Squeezing Unsteady MHD Nanofluid Flow between Parallel Plates with Slip Velocity Effect. *J. Nanosci.* **2016**, *2016*, 9708562. [CrossRef]

13. Siddiqui, A.M.; Irum, S.; Ansari, A.R. Unsteady squeezing flow of a viscous MHD fluid between parallel plates, a solution using the Homotopy Perturbation Method. *Math. Model. Anal.* **2008**, *13*, 565–576. [CrossRef]

14. Hatami, M.; Jing, D.; Song, D.; Sheikholeslami, M.; Ganji, D.D. Heat transferand flow analysis of nanofluid flow between parallel plates inpresence of variable magnetic field using HPM. *J. Magn. Magn. Mater.* **2015**, *396*, 275–282. [CrossRef]

15. Acharya, N.; Das, K.; Kundu, P.K. The squeezing flow of Cu-water and Cu-kerosene nanofluids between two parallel plates. *Alex. Eng. J.* **2016**, *55*, 1177–1186. [CrossRef]

16. Hussain, S.T.; Nadeem, S.; Haq, R.U. Model-based analysis of micropolar nanofluid flow over a stretching surface. *Eur. Phys. J. Plus* **2014**, *129*, 161. [CrossRef]

17. Timofeeva, E.V.; Routbort, J.L.; Singh, D. Particle shape effects on thermophysical properties of alumina nanofluids. *J. Appl. Phys.* **2009**, *106*, 014304. [CrossRef]

18. Vajravelu, K.; Prasad, K.V.; Lee, J.; Lee, C.; Pop, I.; Van Gorder, R.A. Convective heat transfer in the flow of viscous Ag-water and Cu-water nanofluids over a stretching surface. *Int. J. Therm. Sci.* **2011**, *50*, 843–851. [CrossRef]

19. Makinde, O.D.; Aziz, A. Boundary layer flow of a nanofluid past a stretching sheet with a convective boundary condition. *Int. J. Therm. Sci.* **2011**, *50*, 1326–1332. [CrossRef]

20. Sheikholeslami, M.; Ganji, D.D.; Ashorynejad, H.R. Investigation of squeezing unsteady nanofluid flow using ADM. *Powder Technol.* **2013**, *239*, 259–265. [CrossRef]

21. Hu, L.; Harrison, J.D.; Masliyah, J.H. Numerical Model of Electrokinetic Flow for Capillary Electrophoresis. *J. Colloid Interface Sci.* **1999**, *215*, 300–312. [CrossRef] [PubMed]

22. Mala, G.M.; Li, D.; Werner, C.; Jacobasch, H.J.; Ning, Y.B. Flow characteristics of water through a microchannel between two parallel plates with electrokinetic effects. *Int. J. Heat Fluid Flow* **1997**, *18*, 489–496. [CrossRef]

23. Yang, R.J.; Fu, L.M.; Hwang, C.C. Electroosmotic entry flow in a microchannel. *J. Colloid Interface Sci.* **2001**, *244*, 173–179. [CrossRef]

24. Davidson, M.R.; Harvie, D.J.E. Electroviscous effects in low Reynolds number liquid flow through a slit-like microfluidic contraction. *Chem. Eng. Sci.* **2007**, *62*, 4229–4240. [CrossRef]

25. Park, H.M.; Lee, J.S.; Kim, T.W. Comparison of the Nernst–Planck model and the Poisson–Boltzmann model for electroosmotic flows in microchannels. *J. Colloid Interface Sci.* **2007**, *315*, 731–739. [CrossRef] [PubMed]

26. Rojas, G.; Arcos, J.; Peralta, M.; Méndez, F.; Bautista, O. Pulsatile electroosmotic flow in a microcapillary with the slip boundary condition. *Colloids Surf. A Physicochem. Eng. Asp.* **2017**, *513*, 57–65. [CrossRef]

27. Thiyagarajan, P.; Sathiamoorthy, S.; Santra, S.S.; Ali, R.; Govindan, V.; Noeiaghdam, S.; Nieto, J.J. Free and Forced Convective Flow in Pleural Fluid with Effect of Injection between Different Permeable Regions. *Coatings* **2021**, *11*, 1313. [CrossRef]

28. Alam, M.K.; Bibi, K.; Khan, A.; Noeiaghdam, S. Dufour and Soret Effect on Viscous Fluid Flow between Squeezing Plates under the Influence of Variable Magnetic Field. *Mathematics* **2021**, *9*, 2404. [CrossRef]

29. Bilal, S.; Rehman, M.; Noeiaghdam, S.; Ahmad, H.; Akgül, A. Numerical Analysis of Natural Convection Driven Flow of a Non-Newtonian Power-Law Fluid in a Trapezoidal Enclosure with a U-Shaped Constructal. *Energies* **2021**, *14*, 5355. [CrossRef]

30. Ghiasi, E.K.; Noeiaghdam, S. Truncating the series expansion for unsteady velocity-dependent Eyring-Powell fluid. *Eng. Appl. Sci. Lett.* **2020**, *3*, 28–34. [CrossRef]

31. Rizwan, H.; Khan, Z.H.; Hussain, S.H. Flow and heat transfer analysis of Water and Ethylene glycol based Cu nanoparticles between two parallel disks with suction/injection effects. *J. Mol. Liq.* **2016**, *221*, 298–304. [CrossRef]

32. Khan M.S., Rehan A.S., Aamir K. Effect of variable magnetic field on the flow between two squeezing plates. *Eur. Phys. J. Plus* **2019**, *134*, 219. [CrossRef]

33. Khan, M.S.; Rehan, A.S.; Amjad, A.; Aamir, K. Parametric investigation of the Nernst–Planck model and Maxwell's equations for a viscous fluid between squeezing plates. *Bound. Value Probl.* **2019**, *2019*, 107. [CrossRef]

34. Shah, R.A.; Anjum, M.N.; Khan, M.S. Analysis of unsteady squeezing flow between two porous plates with variable magnetic field. *Int. J. Adv. Eng. Manag. Sci.* **2017**, *3*, 239756.

35. Khan, A.; Shah, R.A.; Alam, M.K.; Rehman, S.; Shahzad, M.; Almad, S.; Khan, M.S. Flow dynamics of a time-dependent non-Newtonian and non-isothermal fluid between coaxial squeezing disks. *Adv. Mech. Eng.* **2021**, *13*, 16878140211033370. [CrossRef]

36. Khan, M.S.; Mei, S.; Fern, ez-Gamiz, U.; Noeiaghdam, S.; Shah, S.A.; Khan, A. Numerical Analysis of Unsteady Hybrid Nanofluid Flow Comprising CNTs-Ferrousoxide/Water with Variable Magnetic Field. *Nanomaterials* **2022**, *12*, 180. [CrossRef]

37. Shah, R.A.; Ullah, H.; Khan, M.S.; Khan, A. Parametric analysis of the heat transfer behavior of the nano-particle ionic-liquid flow between concentric cylinders. *Adv. Mech. Eng.* **2021**, *13*, 16878140211024009. [CrossRef]